Decentralized nonlinear robust control for multivariable systems: Application to a 2 DoF laboratory helicopter

Marwa Yousfi[1,*], **Chakib Ben Njima**[1,2], **Tarek Garna**[1,3]

[1] Laboratory of Automatic, Signal and Image Processing, National Engineering School of Monastir, University of Monastir, Ibn El Jazzar Street, 5019 Monastir, Tunisia

[2] Higher Institute of Transport and Logistics of Sousse, University of Sousse, Erriadh city BP 247, 4023 Sousse, Tunisia

[3] Higher Institute of Applied Science and Technology of Sousse, University of Sousse, Ibn Khaldoun city, 4003 Sousse, Tunisia

[*] Corresponding author, marwa.yousfi@enim.rnu.tn

Abstract: In this paper a decentralized nonlinear robust control (DNRC) using loop shaping design procedure (LSDP) and gain scheduling (GS) technique is developed for MIMO (multiple-input/multiple-output) systems. The nonlinear system is linearized in several equilibrium points and for each of these latter a decentralized robust controller is calculated, using a proposed LSDP based on RGA (Relative Gain Array) theory, to regulate the system around the equilibrium point. To do this. The use of RGA theory is exploited to define the structure of the weighting controller of the LSDP with the most effective input/output pairing. Then, for each equilibrium point a full-order robust controller is calculated using LSDP, which configuration is simplified exploiting the RGA theory by proposing a selection matrix to deduce a simplified final robust controller. The overall control system is obtained by GS technique from switching between local simplified final robust controllers according to the scheduling parameter's (SP) value. The proposed algorithm of control is validated on the AERO system of Quanser.

Keywords: Quanser's AERO; MIMO nonlinear systems; RGA theory; robustness; decentralized control; gain scheduling

1 Introduction

MIMO control systems has been always a rich material of research. Due to multiavariable system's loop interactions, this area of research challenged many researchers who have proposed many solutions to deal with loop interactions. Decen-

tralized control and decoupling have been used widely to minimize or compensate loop interactions in MIMO processes and many studies used these two solutions and combined them with other approaches to come up with good control systems for MIMO processes for example in [1], the authors proposed a novel inverted fuzzy decoupling scheme for MIMO systems with disturbance and the case of binary distillation column has been studied. In [2] an adaptive fuzzy decentralized control for a class of large-scale MIMO nonlinear state delay systems with unmodeled dynamics subject to unknown input saturation and infinite number of actuator failures was proposed. A review of the most extensively applied coupling interaction analysis and decoupler design methods for industrial processes is carried out in [3]. In [4], the authors reviewed and proposed a classification of a number of decentralized, distributed and hierarchical control architectures for large scale systems. An analysis and design of robust multivariable control systems focusing on practical feedback control and not on system theory in general is presented in [5]. [6] offers a novel take on advanced control engineering design techniques for wind turbine applications. In [7] a nonlinear intelligent decoupling controller is developed to stabilize the levitation system. The control architecture consists of three components: (1) fuzzy sliding mode technique for the uncertainty in the system parameter; (2) force distribution for decoupling; (3) extended state observer for compensating the system disturbance. However, to manage loop interactions one must quantify them first. In this context, many tools have been proposed in the literature to solve this issue [8, 9]. The RGA theory [10] is one of these tools that offers a simple way of calculating loop interactions and many extensions of this theory have been developed [11, 12, 13].

Recently, considerable attention has been paid to the control design of robots and helicopters specifically due to their potential military and civil applications see for instance [14, 15, 16]. The challenges in controller design for those type of systems originates from their particular characteristics namely nonlinearity, loop interactions and uncertainties. In the last two decades, many works have been reported in the area of control design for flying vehicles. A 2 DoF Helicopter is a typical MIMO nonlinear system with loop interactions. Hence, it is an ideal test bed to verify the effectiveness of various control schemes. In [17], LQR and LQR-I controllers are designed and have been turned out to be powerful in stabilization and also in tracking desired command input. However, controllers in [17] are not able to handle few uncertainties like, unmodeled elements and external disturbances. This requires the design of a robust controller which can handle above difficulties. In [18], the H_∞ loop shaping framework has been extended by applying two methods of compensator synthesis approach for tracking desired pitch and yaw angles of helicopter. The decentralized discrete-time neural control strategy has been presented in [19] to control pitch and yaw angles. A backstepping controller synthesis methodology has been presented in [20]. By suitably combining adaptive control and LQR-I control, a new robust control scheme has been presented in [21]. Furthermore, a multivariable adaptive sliding mode observer based robust control strategy is presented in [22]. From [23], an intelligent proportional–integral (iPI) is proposed using Takagi-Sugeno Fuzzy (TSF) logic for twin rotor aerodynamic systems. In [24] an hybrid PID controller was implemented using FPGA for a real time TRMS

control. Zeghlache and Amardjia proposed in [25] Real time implementation of non linear observer-based fuzzy sliding mode controller for a twin rotor MIMO system (TRMS).

In this paper, we use Quanser 2 DoF laboratory helicopter to investigate the robust stability and tracking control performances of the proposed decentralized nonlinear robust control. A 2 DoF Helicopter is a typical MIMO nonlinear system with cross couplings or process interactions and unmodeled dynamics. Hence,it is an ideal test bed to verify the effectiveness of various control schemes.

Otherwise, LSDP approach [26] is considered as one powerful tool for robust control system design, for handling model uncertainties and bounded external perturbations, that has been proven to be effective in industrial design. This approach involves the robust stabilization of additive perturbations of normalized coprime factors of a shaped plant. Prior to robust stabilization, the open-loop singular values are shaped using a weighting controller to give a desired open-loop shape which corresponds to a good closed-loop performance. The LSDP has attracted many researchers since 19^{th} century, thanks to its simplicity and robustness as a result many theoretical researches and applications has been done [5, 27, 28, 29, 30]. For instance, in [31] the authors proposed a robust loop-shaping control for a nano-positioning stage. A multi-objective differential evolution (MODE)-based extended H-infinity controller for autonomous helicopter has been developed in [32]. A new Suggested Model Reference Adaptive Controller for the Divided Wall Distillation Column is suggested in [33].

However, a successful design using LSDP depends on the appropriate choice of weighting controllers. The selection of these latter is usually done by a trial-and-error method and is based on the designer's experience. Motivated by this fact, we propose the use of RGA theory to decide the structure of the weighting controller to yield a decentralized control structure which minimise loop interaction in a multi-loop context. The obtained LSDP controller will be a full-order matrix that we propose to simplify their structure using the RGA theory again.

In the other hand, most engineering system are non linear. Synthesis of nonlinear control systems interested many researchers. For instance, in [34] an approach to the design of nonlinear state-space control systems is presented. The approach is supported by a geometrical illustration of systems evolution in the state space. In our case, to move to the nonlinear case, we will be using GS technique. The basic idea is to divide the synthesis of a control system to two steps. The first step is the linearization on equilibrium points, which is based on the approximation of the nonlinear system with a set of linear local models computed for a family of fixed values of the SP $\boldsymbol{\rho}$. Then an offline calculation of a controller using linear control strategies is applied to the linearized model at each equilibrium point. The second step, is accomplished by switching or interpolating the local controllers obtained for each operating point. The interpolation/switching is made from a set of SP $\boldsymbol{\rho}$ that capture the change in the system's equilibrium point. Thus, the dynamic behavior of a control system changes with the operating point. The GS technique is widely used to control nonlinear system [35, 36, 37, 38].

1.1 Main contribution

In literature, we precise that to guarantee MIMO process regulation, a several MIMO control approaches were proposed namely the sliding mode control [39, 40] and the adaptive predictive control [41, 42]. Adaptive predictive control is used to deal with some critical parameters in the system structure. In the other hand, sliding mode control deals with uncertainties in rapidly changing parameters and unstructured uncertainties. Then the adaptive predictive control and sliding mode control algorithms allow handling changes in the system's dynamics with respect to parametric uncertainties. Nevertheless, these algorithms don't deal with the input/output interactions problem using multiloop control structure design by exploiting a set of controllers. Consequently, we place ourselves in the so-called decentralized control which have proven its effectiveness compared to the centralized control dealing with the process interactions. Furthermore, because of the process interactions a change in a manipulated variable affects all the controlled variables and it is not always clear which input should be "paired" with which output to synthesize an effective control system. In this regard, we have studied the RGA theory and the LSDP approach which offers the following advantages. The RGA theory is used to quantify the loop interaction in MIMO systems. Thus, it could be made use of to decide the best control structure in a decentralized configuration framework. The LSDP controller tracks desired response quickly with minimum overshoot in presence of parametric uncertainties. However for MIMO systems a full order MIMO controller is obtained and things can gets complicated if the system has many inputs/outputs or important loop interactions. If LSDP approach and RGA theory are combined and a new algorithm is proposed, we can have all the advantages in one algorithm. This thought has motivated us to develop a new robust control algorithm. Thus, we propose the use of RGA theory to decide the structure of the weighting and the final robust controllers of the LSDP approach. To apply the proposed algorithm to nonlinear systems we used GS technique. Therefore, a set LSDP controller is calculated for a predefined number of equilibrium points. The overall controller is obtained by switching between these controllers. To demonstrate the superiority of the proposed controller, experimental results are obtained on a 2 DoF helicopter which is fourth order, two-input/two-output, nonlinear coupled system. The obtained results are quite satisfactory and support the validity of the analysis developed.

1.2 Structure of the paper

This paper is structured as follows: the first section is an introduction, where we present the essential of our work and the main contribution. The second section: 'background' we briefly review the notion of decentralized control and we introduce the RGA theory, then a brief introduction to the LSDP approach. In the third section 'Main results' we propose the use of the RGA theory to decide on the structure of the weighting controller matrix's configuration. Then, the LSDP approach is used to calculate for each equilibrium point a final robust controller. These latter are simplified using RGA theory and a global robust controller is synthesized by exploiting the GS technique. In the fourth section 'Experimental validation: AERO system' the proposed algorithm is tested on a 2 DoF helicopter.

2 Background

In this section we present the notions of decentralized control and RGA theory along with LSDP approach.

2.1 Decentralized control and RGA theory

The decentralized control [43, 44, 45], is based on a multiloop control structure i.e. the use of n SISO controllers to control a multivariable process with n inputs/outputs. Each loop is defined by an input u_j and its associated output y_k. The selection of input/output pairing can be decided using the RGA theory [10]. In fact, for most MIMO systems, each input affects all measured outputs, and it is not always clear which input should be "paired" with which output to calculate the most efficient control. Therefore the RGA theory is a one tool that allows to fix the most effective input/output pairing that allows to minimize loop interactions. Therefore, to minimize undesired interactions, pairings corresponding to a RGA element as close to one as possible should be selected, see for instance [11]. The RGA metric is given by:

$$\boldsymbol{\Lambda} = \boldsymbol{G}(s=0) \odot \boldsymbol{G}^{-T}(s=0) = [\lambda_{jk}]_{1\leq j,k\leq n} \tag{1}$$

such that $\boldsymbol{G}(s=0)$ is the system transfer matrix and "$\odot$" is the Hadamard product (product element by element). Consequently, based on values of λ_{jk}, the configuration of the decentralized controller $\boldsymbol{K}_d(s)$ is decided as follows:

$$\boldsymbol{K}_d(s) : \begin{cases} K_{kj}(s) \neq 0 & if \quad \lambda_{jk} \textit{ is the closest to } 1 \\ K_{kj}(s) = 0 & else \end{cases} \tag{2}$$

2.2 LSDP approach

Many industrial systems are characterized by parametric uncertainties that may occur during their functioning and affect their dynamics. This phenomenon may cause problems specially for systems where parameter's precision is important namely the aeronautical and chemical systems (missiles, planes, batch reactors, CSTR, etc ...) where parameters uncertainties affect adversely the system's functioning. Calculating a controller for this type of systems is not an easy task because these uncertainties must be taken into account in order to obtain efficient control systems, which called robust control. The LSDP developed by [26] is one of these robust control approaches.

The LSDP is based on the exploitation of a filter called weighting controller $\boldsymbol{K}(s)$ to shape the singular values of open loop's transfer matrix $\boldsymbol{G}(s)$. The weighting controller $\boldsymbol{K}(s)$ serves to ameliorate the open loop performances. Typically, it aims to ensure high singular values at low frequencies (to ensure a zero static error in the case of a tracking reference) and low singular values at high frequencies (to ensure robustness against disturbance rejection). In this case, we get the shaped system $\boldsymbol{G}_{sh}(s) = \boldsymbol{G}(s)\boldsymbol{K}(s)$, which can be written in a state space representation [29]:

$$\begin{cases} \dot{\boldsymbol{x}}(t) = \boldsymbol{A}_{sh}\, \boldsymbol{x}(t) + \boldsymbol{B}_{sh}\, \boldsymbol{u}(t) \\ \boldsymbol{y}(t) = \boldsymbol{C}_{sh}\, \boldsymbol{x}(t) + \boldsymbol{D}_{sh}\, \boldsymbol{u}(t) \end{cases} \tag{3}$$

with $\boldsymbol{x}(t) \in R^{m\times 1}$, $\boldsymbol{u}(t) \in R^{n\times 1}$, $\boldsymbol{y}(t) \in R^{p\times 1}$ are the states, inputs and outputs vectors, $\boldsymbol{A}_{sh} \in R^{m\times m}$, $\boldsymbol{B}_{sh} \in R^{m\times n}$, $\boldsymbol{C}_{sh} \in R^{n\times m}$ and $\boldsymbol{D}_{sh} \in R^{n\times n}$ are the state matrices such that pairs of state space matrices $(\boldsymbol{A}_{sh}, \boldsymbol{B}_{sh})$ and $(\boldsymbol{A}_{sh}, \boldsymbol{D}_{sh})$ are respectively controllable and observable with $m \in N^+$ is the order of the system.

Thereafter, [26] proposed the computation of a robust controller $\boldsymbol{K}_\infty(s)$ guaranteeing robust stability against parametric uncertainties. The robust controller is defined as:

$$\boldsymbol{K}_\infty(s) := \left(\begin{array}{c|c} \boldsymbol{A}_{sh} + \boldsymbol{B}_{sh}\boldsymbol{F} + \varepsilon_{max}^{-2}(\boldsymbol{L}^T)^{-1}\boldsymbol{Y}\boldsymbol{C}_{sh}^T(\boldsymbol{C}_{sh} + \boldsymbol{D}_{sh}\boldsymbol{F}) & \varepsilon_{max}^{-2}(\boldsymbol{L}^T)^{-1}\boldsymbol{Y}\boldsymbol{C}_{sh}^T \\ \hline \boldsymbol{B}_{sh}^T\boldsymbol{X} & -\boldsymbol{D}_{sh}^T \end{array}\right) \tag{4}$$

with a maximum stability margin given as :

$$\varepsilon_{max} = (1 + \beta_{max}(\boldsymbol{X}\boldsymbol{Y}))^{-\frac{1}{2}} \tag{5}$$

where the parameters $\boldsymbol{F}$, $\boldsymbol{L}$, $\boldsymbol{Y}$ and $\boldsymbol{X}$ are calculated matrices given in [15]. The final robust Controller $\boldsymbol{K}_f(s)$ is Computed as:

$$\boldsymbol{K}_f(s) = \boldsymbol{K}(s)\boldsymbol{K}_\infty(s) \tag{6}$$

In order to ensure the robust stability of the closed loop system with respect to parameter uncertainties, the following theorems are proposed in the literature:

Theorem 1. [26]
Consider a shaped plant $\boldsymbol{G}_{sh}(s)$ and the stability margin ε_{max}. A robust controller $\boldsymbol{K}_\infty(s)$ stabilizes the uncertain system $\boldsymbol{G}_{sh,\Delta}(s)$:

i). $\boldsymbol{K}_\infty(s)$ stabilizes $\boldsymbol{G}_{sh}(s)$.

ii). $\left\| \begin{bmatrix} \boldsymbol{K}_\infty \\ \boldsymbol{I} \end{bmatrix} (\boldsymbol{I} - \boldsymbol{G}_{sh}\boldsymbol{K}_\infty)^{-1}\tilde{\boldsymbol{K}}_{sh}^{-1} \right\|_\infty \leq \varepsilon^{-1} \quad \text{for all } \varepsilon \leq \varepsilon_{max}$

■

Theorem 2. [27]
Consider a shaped plant $\boldsymbol{G}_{sh}(s)$ and its robust controller $\boldsymbol{K}_\infty(s)$ calculated for the stability margin ε_{max}. Then the following properties are equivalent:

a). The robust controller $\boldsymbol{K}_\infty(s)$ guarantees the closed loop stability of all uncertain systems $\boldsymbol{G}_{sh,\Delta}(s)$ with a stability margin ε_{max}.

b). The robust controller $\boldsymbol{K}_\infty(s)$ stabilizes the uncertain systems $\boldsymbol{G}_{sh,\Delta}(s)$ such as $\delta_g\left(\boldsymbol{G}_{sh}, \boldsymbol{G}_{sh,\Delta}\right) \leq \varepsilon_{\max}$ where δ_g is the gap metric.

■

From Theorems 1 and 2, we note that the robust controller $\boldsymbol{K}_\infty(s)$ obtained by LSDP approach for the shaped system $\boldsymbol{G}_{sh}(s)$ with maximum stability margin ε_{max}, ensures the stabilization of all uncertain systems $\boldsymbol{G}_{sh,\Delta}(s)$. Also, we note a fundamental link between the stability margin ε_{max} and the effect of the stabilization of the robust controller $\boldsymbol{K}_\infty(s)$.

3 Main results

In this section we present the essential of our work: The DNRC.

3.1 LSDP based on RGA theory

At this point, we propose the exploitation of RGA theory with the LSDP approach to develop an algorithm to control nonlinear multivariable uncertain systems guaranteeing both robust stability and reference tracking. The combination of RGA theory with the LSDP approach allows to adjust:

- The weighting controller matrix's configuration.
- The final robust controller matrix's configuration.

The RGA has been selected because it provides a quite simple way of choosing the best input/output pairing configuration to minimize loop interactions. The LSDP controller's configuration must preserve the decentralized control structure defined from RGA theory. Therefore, the LSDP approach can be reformulated as follows:

Step 1 - RGA calculation: given the open loop plant's transfer matrix $\boldsymbol{G}(s)$, calculate $\boldsymbol{\Lambda}$ from (1).

Step 2 - Loop Shaping technique based on RGA theory: to accentuate the most effective input/output pairing based on the RGA theory, we propose to fix the configuration of the weighting controller or the filter of the LSDP as $\boldsymbol{K}_d(s)$ defined in (2). This configuration results from the RGA elements of $\boldsymbol{\Lambda}$ pointed in step 1.

The LS technique provides the shaped system given by:

$$\boldsymbol{G}_{sh}(s) = \boldsymbol{G}(s)\boldsymbol{K}_d(s) \tag{7}$$

Step 3 - Value of $\boldsymbol{K}_d(s)$: typically the designer chooses the elements $K_{kj}(s), j,k = 1,\ldots,n$ as low pass filters in order to have a sufficiently small open-loop singular values in high frequencies in order to assure a good tracking performance with high open-loop singular values in low frequencies to improve noise rejection.

Our next proposition is to exploit the RGA again to simplify the final robust controller $\boldsymbol{K}_f(s)$ calculated using LSDP approach. The proposed simplified final robust controller $\tilde{\boldsymbol{K}}_f(s)$ is determined to emphasize the interaction (u_k/y_j) approved by the RGA theory. Therefore, the simplified final robust controller is calculated:

$$\tilde{\boldsymbol{K}}_f(s) = \boldsymbol{P} \odot \boldsymbol{K}_f(s) \tag{8}$$

where $\boldsymbol{K}_f(s)$ is the final robust controller:

$$\boldsymbol{K}_f(s) = \boldsymbol{K}_d(s)\boldsymbol{K}_\infty(s) = \left[K_{f,kj}(s)\right]_{1\leq j,k\leq n} \tag{9}$$

and $\boldsymbol{P} \in R^{n\times n}$ is a selection matrix determined based on the RGA theory as:

$$\begin{cases} P_{kj} = 1 & if \quad \lambda_{jk} \textit{ is the closest to } 1 \\ P_{kj} = 0 & else \end{cases} \tag{10}$$

3.2 DNRC

We consider a linearization of the system in a set of L equilibrium points, where for each equilibrium point a simplified final robust controller is calculated using LSDP approach. All resulting simplified final robust controllers are interpolated using the GS technique to regulate the nonlinear MIMO system.

Considering a nonlinear continuous-time system described by its ordinary differential equation (ODE) [45, 46]

$$\sum : \begin{cases} \dot{\boldsymbol{x}}(t) = \boldsymbol{f}(\boldsymbol{x}(t), \boldsymbol{u}(t)) \\ \boldsymbol{y}(t) = \boldsymbol{g}(\boldsymbol{x}(t), \boldsymbol{u}(t)) \end{cases} \tag{11}$$

We note that each equilibrium point $(\boldsymbol{x}_{eq}, \boldsymbol{u}_{eq})$ can be defined function of the SP $\boldsymbol{\rho}$ [47, 48]. This latter is fixed as the output vector $\boldsymbol{\rho} = \boldsymbol{y}(t)$. For an equilibrium point $(\boldsymbol{x}_{eq}(\boldsymbol{\rho}), \boldsymbol{u}_{eq}(\boldsymbol{\rho}))$, the functions $\boldsymbol{f}$ and $\boldsymbol{g}$ are approximated to provide the following linear representation:

$$\boldsymbol{G}_{eq}(s) : \begin{cases} \dot{\boldsymbol{x}}(t) = \boldsymbol{A}_{eq}(\boldsymbol{\rho})\, \boldsymbol{x}(t) + \boldsymbol{B}_{eq}(\boldsymbol{\rho})\, \boldsymbol{u}(t) \\ \boldsymbol{y}(t) = \boldsymbol{C}_{eq}(\boldsymbol{\rho})\, \boldsymbol{x}(t) + \boldsymbol{D}_{eq}(\boldsymbol{\rho})\, \boldsymbol{u}(t) \end{cases} \tag{12}$$

where $\boldsymbol{A}_{eq}(\boldsymbol{\rho})$, $\boldsymbol{B}_{eq}(\boldsymbol{\rho})$, $\boldsymbol{C}_{eq}(\boldsymbol{\rho})$ and $\boldsymbol{D}_{eq}(\boldsymbol{\rho})$ are obtained by linearization (or first-order Taylor expansion) of the functions $\boldsymbol{f}$, $\boldsymbol{g}$ at the equilibrium point $(\boldsymbol{x}_{eq}(\boldsymbol{\rho}), \boldsymbol{u}_{eq}(\boldsymbol{\rho}))$ [13].

We precise that we will obtain a set of L simplified final robust controller based on the LSDP approach applied for each equilibrium point. In fact, for each linear transfer matrix $\boldsymbol{G}^i_{eq}(s)$ associated to the i^{th} equilibrium point characterized by the SP $\boldsymbol{\rho}^i$, we compute the shaped system $\boldsymbol{G}^i_{sh}(s)$ using (7), the maximum stability margin ε^i_{max} using (5), the robust controller $\boldsymbol{K}^i_{\infty}(s)$ using (4), the final robust controller $\boldsymbol{K}^i_f(s)$ from (9) and the simplified final robust controller $\tilde{\boldsymbol{K}}^i_f(s)$ by (8) and (10).

The L simplified final robust controllers $\tilde{\boldsymbol{K}}^i_f(s),\ i = 1, \ldots, L$ are used to design a global robust controller $\boldsymbol{K}_{global}(s)$ for the nonlinear system by exploiting the GS technique by switching between the different simplified final robust controllers $\tilde{\boldsymbol{K}}^i_f(s)$ depending on the value of the SP $\boldsymbol{\rho}$ as follows:

$$\boldsymbol{K}_{global}(s) = \begin{cases} \tilde{\boldsymbol{K}}^i_f(s)\ if\ \boldsymbol{\rho}^i \leq \boldsymbol{\rho} < \boldsymbol{\rho}^{i+1},\ i = 1, \ldots, L-1 \\ \tilde{\boldsymbol{K}}^L_f(s)\ if\ \boldsymbol{\rho}^L \leq \boldsymbol{\rho} < \boldsymbol{\rho}^f \end{cases} \tag{13}$$

The proposed DNRC is detailed in algorithm 1.

Algorithm 1 algorithm of synthesis of DNRC system

1. Given a nonlinear system described by its ODE (11), fix the SP $\boldsymbol{\rho}$ as the output vector.
2. Based on the dynamics of the system, fix the equilibrium points $(\boldsymbol{x}^i_{eq}(\boldsymbol{\rho}^i),\ \boldsymbol{u}^i_{eq}(\boldsymbol{\rho}^i)),\ i = 1,\ldots,L$.
3. Using linearization, calculate the state matrices $\boldsymbol{A}^i_{eq},\ \boldsymbol{B}^i_{eq}, \boldsymbol{C}^i_{eq}$ and $\boldsymbol{D}^i_{eq}$ function of SP $\boldsymbol{\rho}$ for each equilibrium point.
4. Based on the RGA metric $\boldsymbol{\Lambda}$, fix the configuration for the future weighting controller matrices $\boldsymbol{K}^i_d(s) = [K^i_{kj}(s)];\ j,k = 1\ldots,n$ associated to the i^{th} equilibrium point and calculate the transfer matrices $\boldsymbol{G}^i_{eq}(s)$ and the shaped transfer matrices $\boldsymbol{G}^i_{sh}(s)$ using (7).
5. Exploit the LSDP approach combined with RGA theory to calculate a robust $\boldsymbol{K}^i_\infty$ using (4) for each equilibrium point.
6. Calculate the final controllers $\boldsymbol{K}^i_f(s),\ i = 1,\ldots,L$ stabilizing $\boldsymbol{G}^i_{sh}(s)$ using (9) for each equilibrium point.
7. Calculate the simplified final robust controller $\tilde{\boldsymbol{K}}^i_f(s),\ i = 1,\ldots,L$ using (8) and (10).
8. Interpolate the L simplified final robust controllers $\tilde{\boldsymbol{K}}^i_f(s),\ i = 1,\ldots,L$, to yield the global robust controller $\boldsymbol{K}_{global}(s)$ by switching between $\tilde{\boldsymbol{K}}^i_f(s),\ i = 1,\ldots,L$ according to the value of SP $\boldsymbol{\rho}$ as described in (13).

Clearly from theorems 1 and 2, at each equilibrium point the robust controller $\boldsymbol{K}^i_\infty$ stabilizes the associated shaped plant $\boldsymbol{G}^i_{sh}$ and we have the performance of the LSDP approach which guarantees the robust stability of the uncertain systems resulting from parameter uncertainties or external perturbation. This robustness property will therefore be reflected in the global robust controller $\boldsymbol{K}_{global}$.

4 Experimental validation: AERO system

The proposed DNRC is practically tested on a TITO system namely the 2 DoF laboratory helicopter: AERO system of Quanser.

4.1 System's description and modeling

The Quanser's AERO, is a fully integrated 2 DoF dual-motor laboratory test platform, designed for control experiments and research for aerospace application. The workstation, consists of an helicopter model mounted on a fixed base with two propellers that are driven by DC motors. The front propeller controls the elevation of the helicopter nose about the pitch axis and the back propeller controls the side to side motions of the helicopter about the yaw axis. The pitch and yaw angles are measured using high resolution encoders. The pitch and yaw encoder and motor

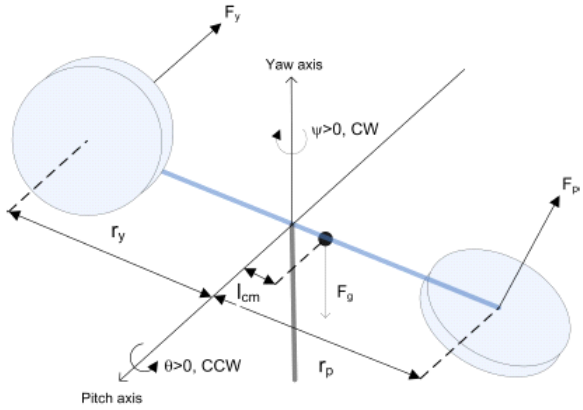

Figure 1
Free-body diagram of the 2 DOF laboratory helicopter

signals are transmitted via a slip ring. This eliminates the possibility of wires tangling on the yaw axis and allows the yaw angle to rotate freely about 360 degrees. However, due to physical limitations, the pitch body is limited to ± 60 degrees. The helicopter setup consists of two degrees of freedom as shown in Figure 1: a motion around the Z axis (yaw), represented by angle ψ, and the rotation around the Y axis (pitch), represented by the angle θ. The input voltages to the DC motors are the control variables and the objective is to control the pitch and yaw angles so as to make the system to track the reference trajectory.

The nonlinear equations of motion of the helicopter system derived using the Euler-Lagrange formula, are as follows :

$$\begin{cases} (J_p + ml^2)\ddot{\theta}(t) = K_{pp}V_{mp}(t) + K_{py}V_{my}(t) + mgl\cos\theta - B_p\dot{\theta}(t) + ml^2\sin\theta\cos\theta\,\dot{\psi}(t)^2 \\ (J_y + ml^2\cos^2\theta)\ddot{\psi}(t) = K_{yp}V_{mp}(t) + K_{yy}V_{my}(t) - B_y\dot{\psi}(t) + 2ml^2\sin\theta\cos\theta\,\dot{\psi}(t)\dot{\theta}(t) \end{cases} \tag{14}$$

where $\theta(t), \dot{\theta}(t), \psi(t), \dot{\psi}(t), F_p, F_y, V_{mp}, V_{my}$ are respectively the pitch angle, pitch velocity, yaw angle, yaw velocity, pitch thrust force, yaw thrust force, control input voltage to pitch and yaw motor. The specifications of various parameters of the system are given in Table 1.

Table 1
AERO Parameters.

Symbol	Description	Value	Unit
J_p	Total moment of inertia about pitch axis	0.0384	$Kg.m^2$
J_y	Total moment of inertia about yaw axis	0.0432	$Kg.m^2$
B_p	Equivalent viscous damping about pitch axis	0.8	N/V
B_y	Equivalent viscous damping about yaw axis	0.318	N/V
K_{pp}	Thrust force constant of yaw motor	0.204	$N.m/V$
K_{yy}	Thrust torque constant of yaw axis from yaw motor	0.072	$N.m/V$
K_{py}	Thrust torque constant acting on pitch axis from yaw motor	0.0068	$N.m/V$
K_{yp}	Thrust torque constant acting on yaw axis from pitch motor	0.0219	$N.m/V$
m	Total moving mass of the helicopter	1.3872	Kg
l	Center of mass length along helicopter body from pitch axis	0.186	m
g	Gravitational acceleration	9.81	m/s^2

The nonlinear equations (14) of the AERO takes the form of (11) with:

$$\boldsymbol{x}(t)=\begin{pmatrix}\theta(t)\\ \psi(t)\\ \dot{\theta}(t)\\ \dot{\psi}(t)\end{pmatrix};\quad \boldsymbol{u}(t)=\begin{pmatrix}V_{mp}(t)\\ V_{my}(t)\end{pmatrix};\quad \boldsymbol{y}(t)=\begin{pmatrix}\theta(t)\\ \psi(t)\end{pmatrix}$$

$$\boldsymbol{f}(\boldsymbol{x}(t),\boldsymbol{u}(t))=\begin{pmatrix}\dot{\theta}(t)\\ \dot{\psi}(t)\\ K_{pp}V_{mp}+K_{py}V_{my}+mgl\cos\theta-B_p\dot{\theta}(t)+ml^2\sin\theta\cos\theta(\dot{\psi}(t))^2\\ K_{yp}V_{mp}+K_{yy}V_{my}-B_y\dot{\psi}(t)+2ml^2\sin\theta\cos\theta\dot{\psi}(t)\dot{\theta}(t)\end{pmatrix}$$

$$\boldsymbol{g}(\boldsymbol{x}(t),\boldsymbol{u}(t))=\begin{pmatrix}\theta(t) & 0 & 0 & 0\\ 0 & \psi(t) & 0 & 0\end{pmatrix} \tag{15}$$

The first step of algorithm 1 is the fixing of the SP $\boldsymbol{\rho}$. We will consider the output vector $\boldsymbol{y}(t)$ as SP:

$$\boldsymbol{\rho}=\begin{pmatrix}\theta_{eq}\\ \psi_{eq}\end{pmatrix} \tag{16}$$

The SP $\boldsymbol{\rho}$ define the equilibrium point $(\boldsymbol{x}_{eq},\boldsymbol{u}_{eq})$ of the nonlinear system (14) and verify:

$$\boldsymbol{f}(\boldsymbol{x}_{eq}(\boldsymbol{\rho}),\boldsymbol{u}_{eq}(\boldsymbol{\rho}))=0 \tag{17}$$

where :

$$\boldsymbol{x}_{eq}=\boldsymbol{\rho}\quad;\quad \boldsymbol{u}_{eq}=\begin{pmatrix}V_{mp,eq}\\ V_{my,eq}\end{pmatrix} \tag{18}$$

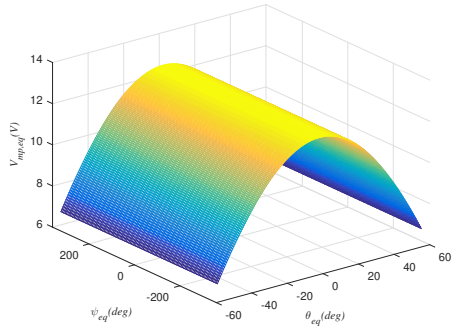

Figure 2
Pitch input voltage function of outputs angles

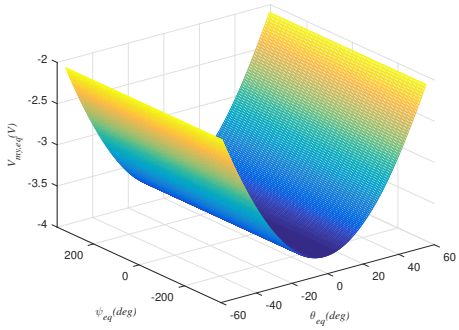

Figure 3
Yaw input voltage function of outputs angles

From (15) and (17) and after calculation, we get:

$$\begin{aligned} V_{mp,eq} &= m\,g\,l\,cos\theta_{eq}\,\frac{K_{yy}}{K_{pp}K_{yy}-K_{py}K_{yp}} \\ V_{my,eq} &= -\frac{K_{yp}}{K_{yy}}\,V_{mp,eq} \end{aligned} \tag{19}$$

The dynamics of the AERO is presented in Figures 2 and 3 where the yaw rotates freely about 360 degrees however the pitch rotation is delimited to ± 60 degrees due to physical constraints so the the operational domain is limited to:

$$\begin{aligned} -60^\circ \leq \theta_{eq} \leq 60^\circ \\ -360^\circ \leq \psi_{eq} \leq 360^\circ \end{aligned} \tag{20}$$

Based on Figures 2 and 3, we notice that the system's dynamics is rather linear for $\theta_{eq} \leq 0$ and $\theta_{eq} > 0$ so we will fix the equilibrium points based on this ascertainment as follows:

$$(\boldsymbol{x}^1_{eq}(\boldsymbol{\rho}^1), \boldsymbol{u}^1_{eq}(\boldsymbol{\rho}^1)) : \begin{cases} \theta^1_{eq} = -60^\circ \\ \psi^1_{eq} = -360^\circ \\ V^1_{mp,eq} = 6.7726\ V \\ V^1_{my,eq} = -2.06\ V \end{cases} ; \; (\boldsymbol{x}^2_{eq}(\boldsymbol{\rho}^2), \boldsymbol{u}^2_{eq}(\boldsymbol{\rho}^2)) : \begin{cases} \theta^2_{eq} = 60^\circ \\ \psi^2_{eq} = -360^\circ \\ V^2_{mp,eq} = 6.7726\ V \\ V^2_{my,eq} = -2.06\ V \end{cases} \tag{21}$$

which constitutes step 2 of algorithm 1 for $L = 2$.

Taking into account (15), the linearization of (14) around an equilibrium point

$(\boldsymbol{x}_{eq}(\boldsymbol{\rho}), \boldsymbol{u}_{eq}(\boldsymbol{\rho}))$ using first-order Taylor expansion is given:

$$\boldsymbol{A}_{eq}(\boldsymbol{\rho}) = \begin{pmatrix} 0 & 0 & 1 & 0 \\ 0 & 0 & 0 & 1 \\ \frac{mgl}{J_p+ml^2}sin\theta_{eq} & 0 & -\frac{B_p}{J_p+ml^2} & 0 \\ \frac{(K_{yp}V_{mp,eq}+K_{yy}V_{my,eq})}{J_y+ml^2cos^2\theta_{eq}}2ml^2sin\theta_{eq}cos\theta_{eq} & 0 & 0 & -\frac{B_y}{J_y+ml^2cos^2\theta_{eq}} \end{pmatrix}$$

$$\boldsymbol{B}_{eq}(\boldsymbol{\rho}) = \begin{pmatrix} 0 & 0 \\ 0 & 0 \\ \frac{K_{pp}}{J_p+ml^2} & \frac{K_{py}}{J_p+ml^2} \\ \frac{K_{yp}}{J_y+ml^2cos^2\theta_{eq}} & \frac{K_{yy}}{J_y+ml^2cos^2\theta_{eq}} \end{pmatrix}; \quad \boldsymbol{C}_{eq}(\boldsymbol{\rho}) = \begin{pmatrix} 1 & 0 & 0 & 0 \\ 0 & 1 & 0 & 0 \end{pmatrix}; \quad \boldsymbol{D}_{eq}(\boldsymbol{\rho}) = \begin{pmatrix} 0 & 0 \\ 0 & 0 \end{pmatrix} \tag{22}$$

which constitutes step 3 of algorithm 1.

4.2 DNR controller

The next step is the decision on the weighting controllers configuration, to do so it is necessary to discuss input/output pairing of the studied AERO. Thus, we calculated the RGA $\boldsymbol{\Lambda}$ of the system using (1) . After variation of the SP $\boldsymbol{\rho} = (\theta_{eq} \quad \psi_{eq})^T$, we notice that $\boldsymbol{\Lambda}$ in all equilibrium points is constant and given as:

$$\boldsymbol{\Lambda} = \begin{pmatrix} 1.0102 & -0.0102 \\ -0.0102 & 1.0102 \end{pmatrix} \tag{23}$$

Therefore, the pairing $(V_{mp}/\theta, V_{my}/\psi)$ is fixed, which means we will amplify the interaction between the voltage V_{mp} and the pitch rotation θ on one hand and the voltage V_{my} and the yaw rotation ψ on the other hand. In this way, based on (2), the weighting controllers $\boldsymbol{K}_d^i(s)$ will take the following form :

$$\boldsymbol{K}_d^i(s) = \begin{pmatrix} K_1^i(s) & 0 \\ 0 & K_2^i(s) \end{pmatrix} \quad for\ i = 1,2 \tag{24}$$

with :

$$\begin{aligned} K_1^i(s) &= \frac{250s^2+15040s+4000}{s^2+100s} \\ K_2^i(s) &= \frac{101s^2+105s+500}{s^2+100s} \end{aligned} \tag{25}$$

As stated in step 4 of algorithm 1, we calculate for each equilibrium point the transfer matrices $\boldsymbol{G}^i_{eq}(s)$. The results are presented in Table 2 along with the local submodels parameters. Afterwards, the shaped systems $\boldsymbol{G}^i_{sh,eq}(s) = \boldsymbol{G}^i_{eq}(s)\ \boldsymbol{K}^i_d(s), i = 1,2$ are calculated.

Table 2
Equilibrium points $(\boldsymbol{x}^i_{eq}, \boldsymbol{u}^i_{eq})$ and their corresponding transfer matrices $\boldsymbol{G}^i_{eq}$.

i	$\begin{pmatrix}\theta^i_{eq}\\ \psi^i_{eq}\end{pmatrix}$	$\begin{pmatrix}V^i_{mp,eq}\\ V^i_{my,eq}\end{pmatrix}$	$\boldsymbol{G}^i_{eq}$	ε^i_{max}
1	$\begin{pmatrix}-60\\ -360\end{pmatrix}$	$\begin{pmatrix}6.7726\\ -2.06\end{pmatrix}$	$\begin{pmatrix}\frac{-2.06}{s^2+9.26s+24.65} & \frac{0.07871}{s^2+9.26s+24.65}\\ \frac{0.3828}{s^2+5.558s} & \frac{1.259}{s^2+5.558s}\end{pmatrix}$	0.4669
2	$\begin{pmatrix}60\\ -360\end{pmatrix}$	$\begin{pmatrix}6.7726\\ -2.06\end{pmatrix}$	$\begin{pmatrix}\frac{2.361}{s^2+9.26s-24.65} & \frac{0.07871}{s^2+9.26s-24.65}\\ \frac{0.3828}{s^2+5.558s} & \frac{1.259}{s^2+5.558s}\end{pmatrix}$	0.4103

Therefore, the nonlinear behavior of the system $\sum$ is described by switching between local models $\boldsymbol{G}^i_{eq}\,; i = 1,2$ according to the SP $\boldsymbol{\rho} = (\theta_{eq}\ \ \psi_{eq})^T$.

$$\sum := \begin{cases} \boldsymbol{G}^1_{eq}\ \ if\ \ -60^\circ \le \theta(t) \le 0^\circ\ and\ -360^\circ \le \psi(t) \le 360^\circ \\ \boldsymbol{G}^2_{eq}\ \ if\ \ 0 < \theta(t) \le 60^\circ\ and\ -360^\circ \le \psi(t) \le 360^\circ \end{cases} \tag{26}$$

Taking into account steps 5, 6 and 7 of algorithm 1, the resulting simplified final robust controllers $\tilde{\boldsymbol{K}}^i_f(s) = \boldsymbol{P} \odot \boldsymbol{K}^i_f(s)$ calculated using (8)-(10) are given by:

$$\tilde{\boldsymbol{K}}^i_f(s) = \begin{pmatrix} K^i_{f_{12}}(s) & 0 \\ 0 & K^i_{f_{21}}(s) \end{pmatrix}; \quad i = 1,2 \tag{27}$$

where $K^i_{f_{12}}(s)$ and $K^i_{f_{21}}(s)$ are calculated and presented in Appendix A using (4) and (6) with $\boldsymbol{P}$ is the selection matrix determined from RGA theory, as detailed in (10):

$$\boldsymbol{P} = \begin{pmatrix} 1 & 0 \\ 0 & 1 \end{pmatrix} \tag{28}$$

Then, as stated in (13) the global robust controller K_{global} of the AERO is constructed by switching between simplified final robust controllers $\tilde{\boldsymbol{K}}^i_f,\ i = 1,2$. According to step 8 of algorithm 1, the switching between the simplified final robust controllers depends on the selection signal I_s which determines the position of the switcher according to the value of SP $\boldsymbol{\rho}$ as detailed as follows:

$$\begin{cases} I_s = 1\ \ and\ \ \boldsymbol{K}_{global} = \tilde{\boldsymbol{K}}^1_f\ \ if\ \ -60^\circ \le \theta(t) \le 0^\circ\ \ and\ \ -360^\circ \le \psi(t) \le 360^\circ \\ I_s = 2\ \ and\ \ \boldsymbol{K}_{global} = \tilde{\boldsymbol{K}}^2_f\ \ if\ \ 0 < \theta(t) \le 60^\circ\ \ and\ \ -360^\circ \le \psi(t) \le 360^\circ \end{cases} \tag{29}$$

The experimental validation was assured thanks Quanser AERO USB experiment. This latter interfaces with Quanser control software QUARC running on a laboratory PC via a standard USB 2.0 connection. The Quanser AERO USB can be used with MATLAB/Simulink and Quanser QUARC software. With the USB version of the experiment, the experimental sheme control represented in Figure 4 is characterized by:

- Quanser Control Software (required for Quanser AERO USB experiment): QUARC for MATLAB/Simulink transfers the control signals V_{mp} and V_{my} generated by the controller and it also allows the acquisition of pitch and yaw angles measured through optical encoders.
- A PC with MATLAB/Simulink and QUARC installed.
- QFLEX 2 USB panel for real time communication with PC.
- Quanser's 2 DoF helicopter: AERO system.

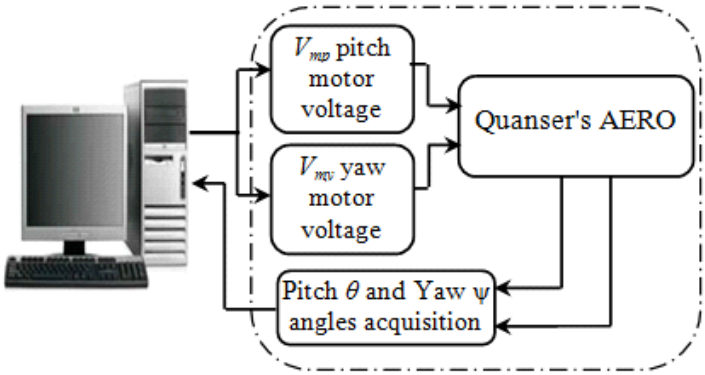

Figure 4
Experimental scheme

Figure 5 shows the the experimental setup. For more informations about the QUARC and the helicopter AERO of QUANSER one can refers to their data-sheets [49, 50]. We precise that, in our case, the sampling time was fixed as $T_e = 0.02s$.

Figures 6, 8 and 10 includes evolution of output and reference signals, control signals and selection indicator I_s respectively.

On examining Figure 6, output signals $\theta(t)$ and $\psi(t)$ are observed to follow the reference signals r_θ and r_ψ respectively. This highlights the good performance of the global controller $\boldsymbol{K}_{global}$ according to the switching between the tho simplified final robust controllers $\tilde{\boldsymbol{K}}_f^i(s)$; $i = 1,2$. These controllers come into play by applying the control by GS technique as a function of the variation scheduling vector $\boldsymbol{\rho}$ controlling the switching from one controller to another. This is illustrated in Figure

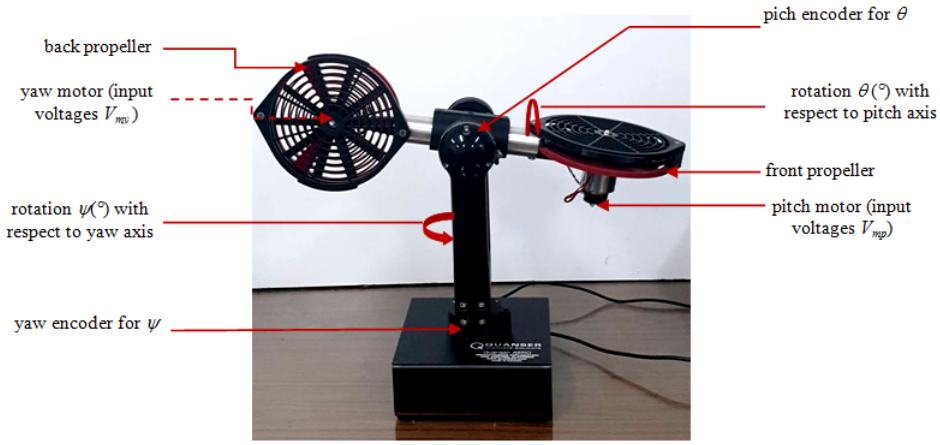

Figure 5
Quanser's AERO System

10 where the selection indicator I_s shows the switching between the simplified final robust controllers which is essential to produce the control signal $\boldsymbol{u}(t)$ presented in Figure 8 guaranteeing the regulation of the AERO system.

Processes are subject to uncertainties in their parameters and perturbations that may affect their dynamics during operation. Therefore, it is worth to investigate the effectiveness of the synthesized controller with such circumstances. To test the robustness of the global controller K_{global}, a manual perturbation is applied to the process to the rotation of the pitch θ while operating to test the reaction of the control. Figures 7, 9 and 11 present the same previous signals with the applied perturbation.

Figure 7 shows that at the moment of the application of the perturbation due to loop interactions, the yaw angle ψ loosed its trajectory but quickly returned to the desired trajectory. This can be seen at Figure 11, such that at the time of the disturbance, we have a variation of the selection indicator I_s in order to switch between the 2 robust controllers $\tilde{\boldsymbol{K}}_f^1(s)$ and $\tilde{\boldsymbol{K}}_f^2(s)$. Therefore, from this switching, we observe from Figure 9 the calculation of new values of control signals V_{mp} and V_{my} in order to compensate and to cope with the manual disturbance. Finally, these Figures shows the robustness of the proposed global robust controller.

5 Conclusion

A DNRC algorithm of control of nonlinear MIMO systems was proposed using LSDP approach combined with RGA theory and GS technique which has been experimentally validated and proved to be a highly effective control strategy for handling model uncertainties and bounded external perturbations. This was clearly demonstrated through the case study using the 2 DoF laboratory helicopter. The

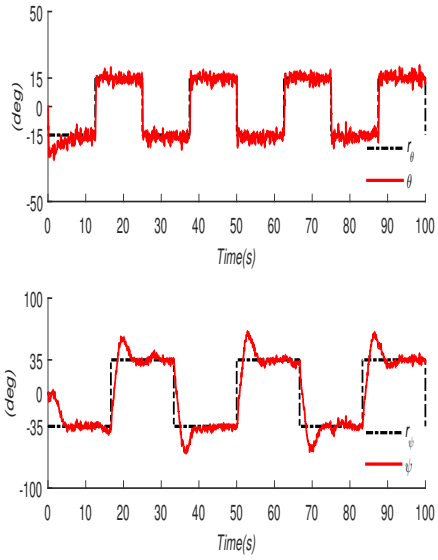

Figure 6
Evolution of output and reference signals without perturbation

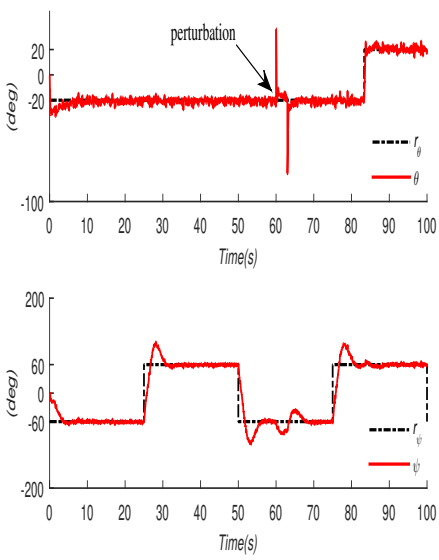

Figure 7
Evolution of output and reference signals with perturbation

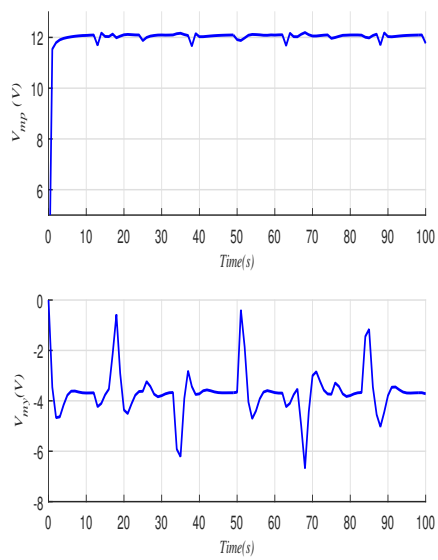

Figure 8
Evolution of control signals without perturbation

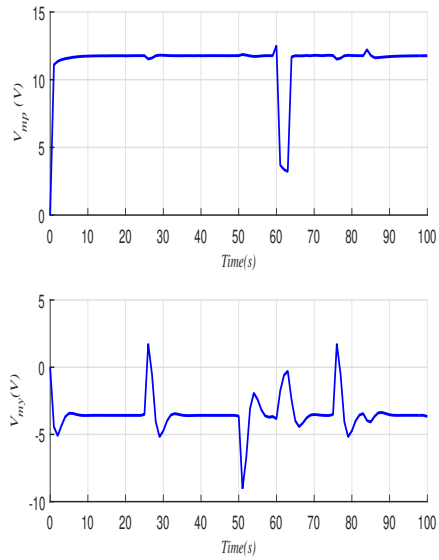

Figure 9
Evolution of control signals with perturbation

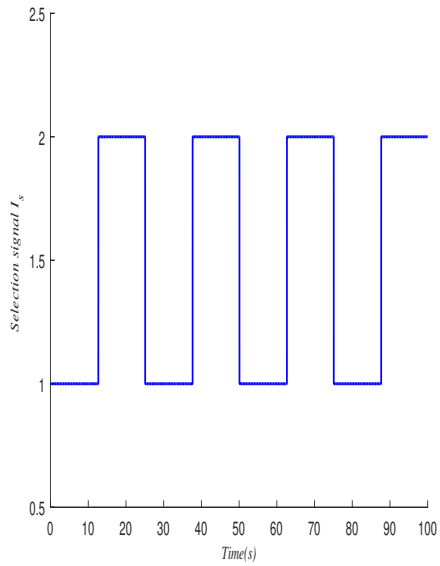

Figure 10
Evolution of the selection indicator I_s without perturbation

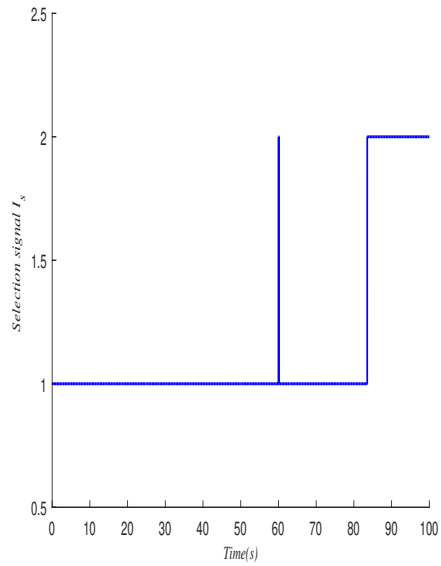

Figure 11
Evolution of the selection indicator I_s with perturbation

results show that the developed control strategy offers good performances in terms of robust stability, reference tracking and perturbation's rejection.

References

[1] Hamdy, M., Ramadan, A. and Abozalam, B. (2018). A novel inverted fuzzy decoupling scheme for MIMO systems with disturbance: a case study of binary distillation column. Journal of Intelligent Manufacturing, 29(8), 1859-1871.

[2] Moradvandi, A., Shahrokhi, M. and Malek, S. A. (2019). Adaptive fuzzy decentralized control for a class of MIMO large-scale nonlinear state delay systems with unmodeled dynamics subject to unknown input saturation and infinite number of actuator failures. Information Sciences, 475, 121-141.

[3] Liu, L., Tian, S., Xue, D., Zhang, T., Chen, Y. and Zhang, S. (2019). A Review of Industrial MIMO Decoupling Control. International Journal of Control, Automation and Systems, 17(5), 1246-1254.

[4] Scattolini, R. (2009). Architectures for distributed and hierarchical model predictive control–a review. Journal of process control, 19(5), 723-731.

[5] Skogstad S and Postlethwaite I (2005) *Multivariable feedback control, Analysis and design*. John Wiley and sons, England.

[6] Houpis, Constantine H, and Garcia-Sanz M (2012). *Wind energy systems: control engineering design*. CRC press.

[7] Zhang J, Mei X, Zhang D, Jiang G and Liu Q (2013). Application of decoupling fuzzy sliding mode control with active disturbance rejection for MIMO magnetic levitation system. Proceedings of the Institution of Mechanical Engineers, Part C: Journal of Mechanical Engineering Science, 227(2), 213-229.

[8] Kinnaert M (1995) *Interaction measures and pairing of controlled and manipulated variables for multiple-input-multiple-output systems: a survey*. Journal A, 36(4), 15-23.

[9] van de Wal M and de Jager B (1995) *Control structure design: A survey*. In American Control Conference, Proceedings (Vol. 1, pp. 225-229). IEEE.

[10] Bristol E (1966) *On a new measure of interaction for multivariable process control*. IEEE transactions on automatic control, 11(1), 133-134.

[11] Khaki-Sedigh A and Moaveni B (2009) *Control configuration selection for multivariable plants* (Vol. 391). Springer.

[12] Halvarsson B (2010). *Interaction Analysis in Multivariable Control Systems: Applications to Bioreactors for Nitrogen Removal* Acta Universitatis Upsaliensis. Uppsala Dissertations from the Faculty of Science and Technology 92. 162 pp. Uppsala. ISBN 978-91-554-7781-3.

[13] Bequette, B. W. (2003). Process control: modeling, design, and simulation. Prentice Hall Professional.

[14] Boza A S, Guerra R H and Gajate A (2011). Artificial cognitive control system based on the shared circuits model of sociocognitive capacities. A first approach. Engineering Applications of Artificial Intelligence, 24(2), 209-219.

[15] Blažič S (2013). On periodic control laws for mobile robots. IEEE transactions on industrial electronics, 61(7), 3660-3670.

[16] Takács Á, Kovács L, Rudas I, Precup R E and Haidegger T (2015). Models for force control in telesurgical robot systems. Acta Polytechnica Hungarica, 12(8), 95-114.

[17] Apkarian J, Levis M, Fulford C (2012). Usermanual of 2-DOF helicopter experiment setup and configuration. Ontario, Canada: Quanser.

[18] Halsey K M and Glover K (2005). Analysis and synthesis of nested feedback systems. IEEE transactions on automatic control, 50(7), 984-996.

[19] Hernandez-Gonzalez M, Alanis A Y and Hernandez-Vargas E A (2012). Decentralized discrete-time neural control for a Quanser 2-DOF helicopter. Applied Soft Computing, 12(8), 2462-2469.

[20] Samadi B and Rodrigues L (2014). A sum of squares approach to backstepping controller synthesis for piecewise affine and polynomial systems. International Journal of Robust and Nonlinear Control, 24(16), 2365-2387.

[21] Nuthi P and Subbarao K (2015). Experimental verification of linear and adaptive control techniques for a two degrees-of-freedom helicopter. Journal of Dynamic Systems, Measurement, and Control, 137(6), 064501.

[22] Khayati K (2015). Multivariable adaptive sliding-mode observer-based control for mechanical systems. Canadian Journal of Electrical and Computer Engineering, 38(3), 253-265.

[23] Roman R C, Precup R E and David R C (2018). Second order intelligent proportional-integral fuzzy control of twin rotor aerodynamic systems. Procedia computer science, 139, 372-380.

[24] Chang C M and Juang J G (2014). Real time TRMS control using FPGA and hybrid PID controller. In 11th IEEE International Conference on Control & Automation (ICCA) (pp. 983-988). IEEE.

[25] Zeghlache S and Amardjia N (2018). Real time implementation of non linear observer-based fuzzy sliding mode controller for a twin rotor multi-input multi-output system (TRMS). Optik, 156, 391-407.

[26] McFarlane D and Glover K (1990) *Robust Controller Design Using Normalized Coprime Factor Plant Descriptions* (Lecture Notes in Control and Information Sciences).

[27] Georgiou T T and Smith M (1990). Optimal Robustness in the Gap Metric, IEEE Transactions on Automatic Control, Vol. 35, 6, 673-686.

[28] Haj Salah A A, Garna T, Ragot J and Messaoud H (2016) *Transition and control of nonlinear systems by combining the loop shaping design procedure and the gap metric theory*. Transactions of the Institute of Measurement and Control, 38(8), 1004-1020.

[29] Pohl, L. and Vesely, I. (2016). Speed control of induction motor using H linear parameter varying controller. IFAC-PapersOnLine, 49(25), 74-79.

[30] Chen, C. L. and Tsai, M. C. (2018). Dynamic Switching of Two Degree-of-Freedom Control for Belt-Driven Servomechanism. IEEE Access, 6, 77849-77858.

[31] Wang F C, Chen L S, Tsai Y C, Hsieh C H and Yen J Y (2014). Robust loop-shaping control for a nano-positioning stage. Journal of Vibration and Control, 20(6), 885-900.

[32] Tijani, I. B., Akmeliawati, R., Legowo, A. and Budiyono, A. (2015). Optimization of an extended H-infinity controller for unmanned helicopter control using Multiobjective Differential Evolution (MODE). Aircraft Engineering and Aerospace Technology: An International Journal, 87(4), 330-344.

[33] El-Gendy, E. M., Saafan, M. M., Elksas, M. S., Saraya, S. F. and Areed, F. F. (2019). New Suggested Model Reference Adaptive Controller for the Divided Wall Distillation Column. Industrial and Engineering Chemistry Research, 58(17), 7247-7264.

[34] Pozna C and Precup R E (2018). An Approach to the Design of Nonlinear State-Space Control Systems. Studies in Informatics and Control, 27(1), 5-14.

[35] Rugh W J and Shamma J S (2000) *Research on gain scheduling*. Automatica, 36(10), 1401-1425.

[36] Kwon H Y and Choi H L (2014). *Gain scheduling control of nonlinear systems based on approximate input-output linearization*. International Journal of Control, Automation and Systems, 12(5), 1131-1137.

[37] Wang Q, Zhou B and Duan G R (2015). Robust gain scheduled control of spacecraft rendezvous system subject to input saturation. Aerospace Science and Technology, 42, 442-450.

[38] Yang Y and Yan Y (2016). Attitude regulation for unmanned quadrotors using adaptive fuzzy gain-scheduling sliding mode control. Aerospace Science and Technology, 54, 208-217.

[39] Ghrab S et al. (2017). Robust discrete-time sliding mode control for systems with time-varying state delay and uncertainties on state and control input. Transactions of the Institute of Measurement and Control, 39(9), 1293-1312. DOI: 10.1177/ 0142331216636954.

[40] Aksu, I. O. and Coban, R. (2019). Sliding mode PI control with backstepping approach for MIMO nonlinear cross-coupled tank systems. International Journal of Robust and Nonlinear Control, 29(6), 1854-1871. DOI: 10.1002/rnc.4469.

[41] Taieb, A., Soltani, M., and Chaari, A. (2017). Parameter Optimization of MIMO Fuzzy Optimal Model Predictive Control By APSO, Hindawi Complexity, Volume 2017, https://doi. org/10.1155/2017/5813192.

[42] Abdelwahed, I. B., Mbarek, A., and Bouzrara, K. (2017). Adaptive MPC based on MIMO ARX-Laguerre model. ISA transactions, 67, 330-347. http://dx.doi.org/10.1016/j.isatra.2016.11.017.

[43] Benhammou A (1988) *Contribution à l'étude de la commande adaptative décentralisée des systèmes interconnectés*. PhD dissertation, Toulouse 3.

[44] Lunze J (1992) *Feedback control of large scale systems*. Prentice Hall International (UK) Ltd, Germany.

[45] Gagnon E (1999) *Commande Algébrique Décentralisée et Multivariable*. Ph.D Thesis, Laval University, Quebec.

[46] Seborg D E, Mellichamp D A, Edgar T F & Doyle III F J (2010). *Process dynamics and control*, third editon. John Wiley & Sons.

[47] Stilwell D J and Rugh W J (2000) *Stability preserving interpolation methods for the synthesis of gain scheduled controllers*. Automatica, 36(5), 665-671.

[48] Leith D J and Leithead W E (1998) *Gain-scheduled controller design: an analytic framework directly incorporating non-equilibrium plant dynamics*. International Journal of Control, 70(2), 249-269.

[49] Quanser (2019). Quanser QUARC Data Sheet. https://quanserinc.app.box.com/s/gvsu5i63ytchc7z2zf0xpnrc9yib1wjs. Ontario, Canada: Quanser.

[50] Quanser (2019). Quanser QUARC Data Sheet. https://quanserinc.box.com/shared/static/bkcgcyo1sl02r1a2mnvhg0zn4cec6m8j.pdf. Ontario, Canada: Quanser.

A Robust Controllers

$$K^1_{f,11}(s) = \frac{4.327\,e^7s^8 + 4.475\,e^9s^7 + 1.978\,e^{11}s^6 + 3.618\,e^{12}s^5 + 2.851\,e^{13}s^4}{731s^9 + 1.828\,e^5s^8 + 2.108\,e^7s^7 + 1.185\,e^9s^6 + 3.033\,e^{10}s^5 + 3.022\,e^{11}s^4} \\ \frac{+9.087\,e^{13}s^3 + 1.42\,e^{14}s^2 + 6.264\,e^{13}s + 8.192\,e^{12}}{+9.913\,e^{11}s^3 + 1.85\,e^{12}s^2 + 4.293\,e^{11}s}$$

$$K^1_{f,22}(s) = \frac{3.404\,e^6s^8 + 3.668\,e^8s^7 + 1.813\,e^{10}s^6 + 3.978\,e^{11}s^5 + 2.279\,e^{12}s^4}{731s^9 + 1.828\,e^5s^8 + 2.108\,e^7s^7 + 1.185\,e^9s^6 + 3.033\,e^{10}s^5 + 3.022\,e^{11}s^4} \\ \frac{+4.853\,e^{12}s^3 + 1.024\,e^{13}s^2 + 5.699\,e^{12}s + 8.733\,e^{11}}{+9.913\,e^{11}s^3 + 1.85\,e^{12}s^2 + 4.293\,e^{11}s} \tag{30}$$

$$K^2_{f,11}(s) = \frac{4.467\,e^7s^8 + 4.767\,e^9s^7 + 2.235\,e^{11}s^6 + 4.599\,e^{12}s^5 + 4.246\,e^{13}s^4}{660.4s^9 + 1.587^5s^8 + 1.813\,e^7s^7 + 1.035\,e^9s^6 + 2.78\,e^{10}s^5 + 3.023\,e^{11}s^4} \\ \frac{+1.595\,e^{14}s^3 + 2.425\,e^{14}s^2 + 9.24\,e^{13}s + 1.021\,e^{13}}{+1.05\,e^{12}s^3 + 2.143\,e^{12}s^2 + 5.033\,e^{11}s}$$

$$K^2_{f,22}(s) = \frac{2.68\,e^6s^8 + 3.447\,e^8s^7 + 2.002\,e^{10}s^6 + 4.725\,e^{11}s^5 + 2.745\,e^{12}s^4}{660.4s^9 + 1.587\,e^5s^8 + 1.813\,e^7s^7 + 1.035\,e^9s^6 + 2.78\,e^{10}s^5 + 3.023\,e^{11}s^4} \\ \frac{+5.871\,e^{12}s^3 + 1.244\,e^{13}s^2 + 7.04\,e^{12}s + 1.092\,e^{12}}{+1.05\,e^{12}s^3 + 2.143\,e^{12}s^2 + 5.033\,e^{11}s} \tag{31}$$